LAWRENCE
LIVERMORE
NATIONAL
LABORATORY

LLNL-PROC-654235

Progress towards Inertial Confinement Fusion Ignition on the National Ignition Facility

D. S. Clark

May 9, 2014

NEDPC 2013
Livermore, CA, United States
March 10, 2014 through March 14, 2014

Disclaimer

Progress towards Inertial Confinement Fusion Ignition on the National Ignition Facility (U)

D. S. Clark, M. J. Edwards (ICF Program Leader),1 P. A. Adams,1 J. B. Alfonso,1 E. T. Alger,1 Z. Alherz,1 L. F. Alvarez,1 S. S. Alvarez,1 P. V. Amick,1 K. S. Andersson,1 S. D. Andrews,1 G. J. Antonini,1 P. A. Arnold,1 D. P. Atkinson,1 L. Auyang,1 S. G. Azevedo,1 B. N. M. Balaoing,1 J. A. Baltz,1 F. Barbosa,1 G. W. Bardsley,1 D. A. Barker,1 A. I. Barnes,1 A. Baron,1 R. G. Beeler,1 B. V. Beeman,1 L. R. Belk,1 J. C. Bell,1 P. M. Bell,1 R. L. Berger,1 M. A. Bergonia,1 L. J. Bernardez,1 L. V. Berzins,1 R. C. Bettenhausen,1 L. Berzak-Hopkins,1 L. Bezerides,1 D. L Bleuel,1 S. D. Bhandarkar,1 C. L. Bishop,1 E. J. Bond,1 D. R. Bopp,1 J. A. Borgman,1 J. R. Bower,1 G. A. Bowers,1 M. W. Bowers,1 D. T. Boyle,1 D. K. Bradley,1 J. L. Bragg,1 J. Braucht,1 D. L. Brinkerhoff,1 D. F. Browning,1 G. K. Brunton,1 S. C. Burkhart,1 S. R. Burns,1 K. E. Burns,1 B. Burr,1 L. M. Burrows,1 R. K. Butlin,1 J. A. Caggiano,1 N. J. Cahayag,1 D. A. Callahan,1 P. S. Cardinale,1 R. W. Carey,1 J. W. Carlson,1 A. D. Casey,1 C. Castro,1 J. R. Celeste,1 C. J. Cerjan,1 G. W. Collins,1 A. Y. Chakicherla,1 F. W. Chambers,1 C. Chan,1 H. Chandrasekaran,1 C. Chang,1 R. F. Chapman,1 K. Charron,1 Y. Chen,1 M. J. Christensen,1 A. J. Churby,1 T. J. Clancy,1 B. D. Cline,1 L. C. Clowdus,1 D. G. Cocherell,1 F. E. Coffield,1 S. J. Cohen,1 R. L. Costa,1 J. R. Cox,1 G. M. Curnow,1 M. J. Dailey,1 P. M. Danforth,1 R. Darbee,1 P. S. Datte,1 J. A. Davis,1 G. A. Deis,1 R. D. Demaret,1 E. L. Dewald,1 P. Di Nicola,1 J. M. Di Nicola,1 T. R. Dittrich,1 L. Divol,1 S. Dixit,1 D. B. Dobson,1 T. Doppner,1 J. D. Driscoll,1 J. Dugorepec,1 J. J. Duncan,1 P. C. Dupuy,1 R. Dylla-Spears,1 E. G. Dzenitis,1 M. J. Eckart,1 S. L. Edson,1 G. J. Edwards,1 O. D. Edwards,1 P. W. Edwards,1 J. C. Ellefson,1 C. H. Ellerbee,1 G. V. Erbert,1 C. M. Estes,1 W. J. Fabyan,1 J. E. Fair,1 R. N. Fallejo,1 M. Fedorov,1 B. Felker,1 J. T Fink,1 M. D. Finney,1 L. F. Finnie,1 M. J. Fischer,1 J. M. Fisher,1 B. T. Fishler,1 J. W. Florio,1 A. Forsman,1 C. B. Foxworthy,1 R. M. Franks,1 T. Frazier,1 G. Frieder,1 T. Fung,1 G. N. Gawinski,1 C. R. Gibson,1 E. Giraldez,1 S. M. Glenn,1 B. P. Golick,1 H. Gonzales,1 S. A. Gonzales,1 M. J. Gonzalez,1 K. L. Griffin,1 J. Grippen,1 G. P. Grim, 2 S. M. Gross,1 P. H. Gschweng,1 G. Gururangan,1 K. Gu,1 S. W. Haan,1 S. R. Hahn,1 B. J. Haid,1 J. E. Hamblen,1 B. A. Hammel,1 A. V. Hamza,1 D. L. Hardy,1 D. R. Hart,1 R. G. Hartley,1 S. P. Hatchett,1 C. A. Haynam,1 G. M. Heestand,1 M. R. Hermann,1 G. L. Hermes,1 D. S. Hey,1 R. L. Hibbard,1 D. G. Hicks,1 D. E. Hinkel,1 D. L. Hipple,1 J. D. Hitchcock,1 D. D. Ho,1 D. L. Hodtwalker,1 J. P. Holder,1 J. D. Hollis,1 G. M. Holtmeier,1 D. M. Holunga,1 J. B. Horner,1 W. W. Hsing,1 H. Huang,1 S. R. Huber,1 A. W. Huey,1 D. N. Hulsey,1 S. L. Hunter,1 T. R. Huppler,1 O. A. Hurricane,1 M. S. Hutton,1 N. Izumi,1 J. L. Jackson,1 M. A. Jackson,1 K. S. Jancaitis,1 D. R. Jedlovec,1 B. Johnson,1 M. C. Johnson,1 T. Johnson,1 M. P. Johnston,1 O. S. Jones,1 D. H. Kalantar,1 J. H. Kamperschroer,1 R. L. Kauffman,1 G. A. Keating,1 L. M. Kegelmeyer,1 S. L. Kenitzer,1 J. R. Kimbrough,1 K. King,1 R. K. Kirkwood,1 J. L. Klingmann,1 K. M. Knittel,1 T. R. Kohut,1 K. G. Koka,1 B. Kozioziemski,1 S. W. Kramer,1 J. E. Krammen,1 K. G. Krauter,1 G. W. Krauter,1 E. K. Krieger,1 A. L. Kritcher,1 J. J. Kroll,1 K. N. La Fortune,1 L. J. Lagin,1 V. K. Lakamsani,1 O. L. Landen,1 S. W. Lane,1 A. B. Langdon,1 S. H. Langer,1 N. Lao,1 D. W. Larson,1 D. Latray,1 G. T. Lau,1 S. Le Pape,1 B. L. Lechleiter,1 Y. Lee,1 T. L. Lee,1 J. Li,1 J. A. Liebman,1 J. D. Lindl,1 S. F. Locke,1 H. K. Loey,1 R. A. London,1 F. J. Lopez,1 D. M. Lord,1 R. R. Lowe-Webb,1 J. G. Lown,1 A. P. Ludwigsen,1 N. W. Lum,1 R. R. Lyons,1 T. Ma,1 B. J. MacGowan,1 A. J. MacKinnon,1 M. D. Magat,1 D. T. Maloy,1 T. N. Malsbury,1 E. Mapoles,1 G. Markham,1 R. M. Marquez,1 A. A. Marsh,1 C. D. Marshall,1 S. R. Marshall,1 I. L. Maslennikov,1 D. G. Mathisen,1 G. J. Mauger,1 M. -Y. Mauvais,1 J. A. McBride,1 T. McCarville,1 J. B. McCloud,1 A. McGrew,1 B. McHale,1 A. G. MacPhee,1 J. F. Meeker,1 N. B. Meezan,1 J. S. Merill,1 E. P. Mertens,1 P. A. Michel,1 M. G. Miller,1 T. Mills,1 J. L. Milovich,1 R. Miramontes,1 R. C. Montesanti,1 M. M. Montoya,1 J. Moody,1 J. D. Moody,1 M. Moran,1 J. C. Moreno,1 K. A. Moreno,1 J. Morris,1 K. M. Morriston,1 D. H. Munro,1 S. R. Nagel,1 B. R. Nathan,1 J. R. Nelson,1 M. Neto,1 J. D. Neumann,1 E. Ng,1 Q. M. Ngo,1 B. L. Olejniczak,1 C. D. Orth,1 N. L. Orsi,1 M. W. Owens,1 E. H. Padilla,1 T. M. Pannell,1 T. G. Parham,1 R. W. Patterson, Jr.,1 A. Pak,1 P. K. Patel,1 G. Pavel,1 D. Pendlton,1 F. A. Penko,1 J. L. Peterson,1 B. L. Pepmeier,1 D. E. Petersen,1 T. W. Phillips,1 D. Pigg,1 K. W. Piston,1 K. D. Pletcher,1 C. L. Powell,1 R. R. Prasad,1 H. B. Radousky,1 B. S. Raimondi,1 J. E. Ralph,1 R. L. Rampke,1 R. K.

Reed,1 W. A. Reid,1 V. V. Rekow,1 B. A. Remington,1 J. L. Reynolds,1 J. J. Rhodes,1 M. J. Richardson,1 R. J. Rinnert,1 B. P. Riordan,1 A. S. Rivenes,1 A. T. Rivera,1 C. J. Roberts,1 H. F. Robey,1 J. A. Robinson,1 R. B. Robinson,1 S. R. Robison,1 O. R. Rodriguez,1 S. P. Rogers,1 M. D. Rosen,1 G. F. Ross,1 J. Steven Ross,1 M. Runkel,1 A. S. Runtal,1 J. R. Rygg,1 R. A. Sacks,1 J. Sater,1 S. F. Sailors,1 J. T. Salmon,1 J. D. Salmonson,1 R. L. Saunders,1 J. R. Schaffer,1 T. M. Schindler,1 M. J. Schmitt,1 M. B. Schneider,1 K. S. Segraves,1 M. J. Shaw,1 M. E. Sheldrick,1 R. T. Shelton,1 M. K. Shiflett,1 S. J. Shiromizu,1 M. Shor,1 L. L. Silva,1 S. A. Silva,1 K. M. Skulina,1 V. A. Smalyuk,1 D. A. Smauley,1 B. E. Smith,1 L. K. Smith,1 A. L. Solomon,1 S. Sommer,1 J. G. Soto,1 N. I. Spafford,1 B. K. Spears,1 D. E. Speck,1 P. T. Springer,1 M. Stadermann,1 F. Stanley,1 T. G. Stone,1 E. A. Stout,1 P. L. Stratton,1 R. J. Strausser,1 L. J. Suter,1 W. Stoeffl,1 W. Sweet,1 M. F. Swisher,1 J. D. Tappero,1 J. B. Tassano,1 J. S. Taylor,1 E. A. Tekle,1 C. Thai,1 C. A. Thomas,1 A. Thomas,1 A. L. Throop,1 G. L. Tietbohl,1 J. M. Tillman,1 R. P. J. Town,1 S. L. Townsend,1 K. L. Tribbey,1 D. Trummer,1 J. Truong,1 J. Vaher,1 M. Valadez,1 P. Van Arsdall,1 A. J. Van Prooyen,1 E. O. Vergel de Dios,1 M. D. Vergino,1 S. P. Vernon,1 J. L. Vickers,1 G. T. Villanueva,1 M. A. Vitalich,1 S. A. Vonhof,1 F. E. Wade,1 R. J. Wallace,1 C. T. Warren,1 A. L. Warrick,1 C. Walters,1 J. Watkins,1 S. Weaver,1 P. J. Wegner,1 M. A. Weingart,1 J. Wen,1 K. S. White,1 P. K. Whitman,1 K. Widmann,1 C. C. Widmayer,1 K. Wilhelmsen,1 E. A. Williams,1 W. H. Williams,1 L. Willis,1 E F. Wilson,1 B. A. Wilson,1 M. C. Witte,1 K. Work,1 P. S. Yang,1 B. K. Young,1 K. P. Youngblood,1 R. A. Zacharias,1 T. Zaleski,1 P. G. Zapata,1 H. Zhang,1 J. S. Zielinski,1 H. W. Herrmann,2 J. L. Kline,2 G. A. Kyrala,2 R. E. Olson,2 A. N. Simakov,2 D. C. Wilson,2 A. Yi,2 R. C. Leepr,3 J. D. Kilkenny,4 A. Nikroo,4 C. Niemann,5 V. Glebov,6 James P. Knauer,6 S. P. Regan,6 T. C. Sangster,6 L. J. A. Frenje,7 M. Gatu Johnson,7 R. Petrasso,7 H. Rinderknecht,7 A.Zylstra,7 A. S. Moore,8 B. M. Van Wonterghem,1 L. J. Atherton,1 and E. I. Moses1

1 Lawrence Livermore National Laboratory, Livermore, California 94550, USA,

2 Los Alamos National Laboratory, Los Alamos, New Mexico 87545, USA,

3 Sandia National Laboratory, Sandia, New Mexico 87185, USA,

4 General Atomics, San Diego, California 92121 , USA,

5 University of California Los Angeles, CA, USA

6 Laboratory for Laser Energetics, University of Rochester, Rochester, New York 14623, USA,

7 Plasma Fusion and Science Center, Massachusetts Institute of Science and Technology, Cambridge, Massachusetts 02139, USA,

8 Atomic Weapons Establishment, Aldermaston, RG7, UK

The National Ignition Campaign (NIC) was completed in September of 2012 with nearly three dozen cryogenic DT ignition experiments fired. While ignition was not achieved in these experiments, substantial progress was made towards that goal: implosion velocities of ~350 km/s were reached, compressions to densities greater than 800 g/cm^3 were achieved, stagnation pressures of more than 100 Gbar were produced, and the ability precisely to control both the temporal sequencing of the implosion and its low-order spatial symmetry were also demonstrated. At present, larger than anticipated low-order asymmetries and possibly larger than expected ablation front instability growth are believed to have been responsible for preventing ignition during the NIC. To address these problems, various exploratory campaigns are now underway to better understand the performance of NIC targets in terms of hydrodynamic stability, hohlraum symmetry, and hohlraum coupling, among others. Simultaneously, alternate ignition designs are being investigated using different ablator materials and different hohlraum configurations. This paper summarizes the results learned from the NIC and current and future experiments planned for understanding and improving implosion performance to the levels necessary for achieving ignition. (Unclassified)

Introduction

The National Ignition Campaign (NIC)[1] on the National Ignition Facility (NIF)[2] represented a collaboration of several hundred scientists and engineers from nearly a dozen institutions, both nationally and internationally, to achieve the long sought-for goal of inertial confinement fusion (ICF) ignition[3] at the laboratory scale. The author list alone should testify to the highly collaborative character of the complex experiments performed during the NIC. For its part, the level of the technical challenge presented in achieving fusion ignition at the energy scale available with NIF (1.8 MJ and 500 TW) is perhaps best illustrated by Fig. 1.

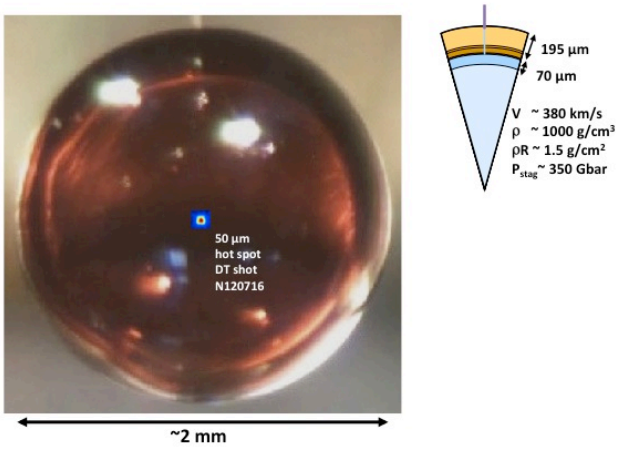

Fig. 1. Schematic illustration of th ehight convergence required to achieve ignition at the NIF energy scale

The figure shows a prototype plastic (CH) ablator NIF capsule of roughly 2 mm outer radius. As summarized in the "pie diagram" to the right, this ~ 200 µm thick CH shell with an inner ~ 70 µm DT ice payload is to be imploded at a peak implosion velocity of ~ 380 km/s to reach an areal density (ρR) of ~ 1.5 g/cm^2 and stagnation pressures of ~ 350 Gbar, conditions suitable to achieve propagating thermonuclear burn. Overlaid on this image is a false-color x-ray image of the ~ 50 µm hot spot from NIF shot N120716 (fired July 16, 2012). The very high convergence ratio of this implosion ($C_R \geq 40$) is apparent. Such a high convergence ratio is the direct consequence of the need to achieve the fixed ignition conditions for DT fusion but at the finite energy scale available on NIF. More importantly, this high level of convergence must be achieved without loosing control of the implosion symmetry or without undue growth of hydrodynamic instabilities or mix over the course of the implosion. Managing these degradation mechanisms in the demanding, high-velocity, high-convergence implosions necessary for ignition on NIF represents the fundamental challenge to be met during the NIC.

Significant progress was made during the NIC towards the goal of ignition: The world's largest and most powerful laser (192 beams, 1.8 MJ, and 500 TW) was brought into routine operation. A diverse suite of diagnostics was commissioned to diagnose implosion performance. A range of highly complex, high-precision targets was fielded, including DT-filled, cryogenic ignition targets with ice layer qualities consistently better than ignition specifications. Shock timing measurements and measurements of implosion symmetry with unparalleled precision in space and time were conducted and shown to improve implosion performance. And finally, nearly three dozen, DT-layered ignition implosion experiments were performed exploring a range target, laser pulse shape, and other fielding parameters in an effort to improve performance. Nevertheless, the ultimate goal of ignition was not achieved by the conclusion of the NIC in September 2012. This paper summarizes the progress made during the NIC, our current understanding of the reasons that ignition was not achieved by the end of the NIC, and a sketch of plans going forward to address these remaining challenges in reaching ignition.

Progression of the National Ignition Campaign

As already summarized in the previous section, considerable progress was made over the course of the NIC toward the ignition goals set for NIF. Quantitatively, DT implosion experiments during the NIC reached stagnated fuel densities of 500 – 800 g/cm^3, fuel areal densities of ~ 1.3 g/cm^2, and inferred stagnation pressures[4] of ~ 150 Gbar.

Comparing to the ignition goals summarized in Fig. 1, this represents encouraging progress with nearly 80% of the intended density and areal density goals achieved, although the inferred stagnation pressure is somewhat lower compared to the goal. Of course, each of these ignition criteria must be achieved simultaneously with the others. Unfortunately, however, during the NIC, these peak values could not be achieved simultaneously: implosions with the highest confinement or areal densities showed lower inferred stagnation pressures and vice versa.

The progression of the NIC over time is summarized in Fig. 2 where implosion performance is plotted in the plane of neutron yield vs. fuel areal density. Here the blue symbols represent the "low foot" shots fired during the NIC, and the green symbols represent "high foot" shots since the NIC and discussed below. The contours indicated yield amplification expected due to α-particle heating. The first cryogenic implosion experiment was carried out on NIF on Sept. 29, 2010[5]. This shot was conducted prior to any of the planned implosion tuning experiments meant empirically to adjust the implosion shock timing and low-mode implosion symmetry[6]. Given that the implosion design codes were not expected to be accurate enough to predict these tuning parameters *a priori* and experimental campaigns were planned to conduct this tuning empirically, it was not surprising that the performance of this first implosion was relatively poor. Note that this commissioning shot used deliberately duded fuel where the optimal 50-50 DT mixture is replaced by an equal-density mixture of predominantly hydrogen (protium) and tritium[7]. As plotted in Fig. 2, the yield has been scaled to represent the performance of this shot as if it had had the optimal DT mixture.

Following the tuning campaigns conducted over the winter of 2010 and the spring and summer of 2011, implosion performance was notably improved. This tuning cycle culminated in the shot fired Sept. 14, 2011 using 1.6 MJ and 430 TW peak laser power (N110914)[8]. Importantly, this implosion also used silicon as a dopant in the CH ablator shell as opposed to the germanium used in the initial round of NIC experiments. This dopant is required to manage the preheating of the implosion by hard x-rays from the surrounding hohlraum, and silicon had been found to accomplish the same preheat control as germanium but while enabling higher implosion velocities. While N110914 represented a substantial improvement in both yield and ρR—moving diagonally through the space in Fig. 2—, a number of succeeding fine adjustments to the low-mode implosion shape[9] did not succeeded in substantially improving the implosion yield or ρR beyond ~ 5×10^{14} and ~ 0.8 g/cm^2, respectively.

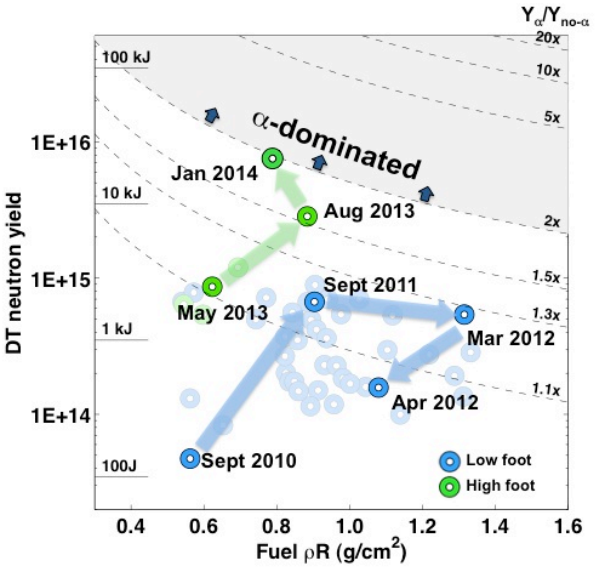

Fig. 2. Progress in NIC implosion performance plotted in the plane of yield vs. confinement

At this point in the NIC, it was decided to pursue higher areal density implosions as a piecewise step towards ignition before pursuing deliberately higher yield implosions. In Fig. 2, this represents a progression horizontally to the right before proceeding upward toward higher yield. Experimentally, a sequence of shots was then fired in which the rise rate to peak laser power was varied and the overall duration of peak laser power was increased. It was found experimentally during this phase of the campaign that slower rise rates ("3 ns rise" as opposed to the earlier "2 ns rise") and a longer duration of laser pulse but at reduced peak power ("no coast implosions" as opposed to earlier "coasters") could increase imploded areal density by ~ 50%. Also during this time, the dopant concentration in the CH ablator shell was increased from 2 to 4 at. % at peak ("2X dopant" as opposed to

the previous "1X dopant"). This was done out of concern that fine-scale mixing was occurring between the CH ablator and DT fuel in flight but conversely was known to endanger the implosion to instability growth at the ablation front[10]. This phase of the campaign culminated in shot N120321[11] (1.5 MJ, 330 TW) fired March 21, 2012 and reaching an areal density of 1.3 g/cm^2 and yield of 4×10^{14}.

From this vantage point of the NIC implosion platform reaching areal densities of nearly 90% of the design goal of 1.5 g/cm^2, the campaign returned to the aim of increasing implosion yield. The most direct means of increasing yield is to increase the implosion velocity or, in turn, to increase the laser power. Several experiments were conducted varying hohlraum parameters relative to N120321 including a high power companion, fired April 5, 2012. This shot used 1.6 MJ and a peak laser power of 390 TW with the hope of achieving a high areal density implosion also with high yield. Unfortunately, the results of this experiment showed a significant drop in both yield and compression. The NIC concluded in September 2012 without achieving the intended combination of both high compression, as shown with N120321, and higher neutron yield.

In parallel to the experimental campaign conducted during NIC, a concerted effort was also undertaken to model NIC experiments in as much detail as possible[12,13] using the HYDRA radiation hydrodynamics code[14]. These simulations were run in a manner similar to the simulations used in designing the original ignition point design but included as much as possible any variations in the target geometry or laser drive particular to a given experiment. Across the full range of pulse shapes and target geometries explored during NIC, these detailed post-shot simulations consistently over-predicted implosion yields by factors from 3 – 10. Given residual uncertainties in the experimental conditions, the simulations could be adjusted within those uncertainties to match approximately the measured areal densities, ion temperatures, and x-ray images sizes, among other properties, but the discrepancy in yield was consistent. This applied even in the case of state-of-the-art, high-resolution, 3-D simulations.

Sources of performance degradation identified since the NIC

During the later phases of the NIC, several hypotheses were developed to explain the observed discrepancies between experimental and simulated implosion performance. A number of effects have been considered, but two leading candidates emerge: larger than anticipated low-mode asymmetries in the imploded fuel configuration and higher than expected levels of ablation front instability growth and subsequent mix of ablator material or cold DT fuel into the hot spot. In the year following the NIC, dedicated NIF experiments were conducted in an attempt to quantify the role played by these effects and strategies for mitigating them. This section describes the evidence for shape and mix failure modes and the experiments conducted to quantify them. The following section describes some of the revised implosion designs being explored to mitigate these sources of performance degradation.

The first clear indication of larger than expected low-mode distortions in the imploded fuel configuration derived from nuclear activation measurements using zirconium threshold detectors. These measurements used seventeen zirconium "pucks" placed around the target chamber to record the neutron fluence in each of these seventeen directions. Where the activation recorded by a puck is high, the scattering of the neutrons emitted by an assumed central source must be low and the corresponding fuel areal density must be low. Conversely, where the activation is low, the scattering must be large and the areal density high. Although the coverage of the 4π steradians of the target chamber is sparse with only seventeen sampling points, it is possible to fit the activation data to a second order Legendre decomposition and from this infer the low-mode fuel asymmetry averaged over the burn duration. Such fits are consistent with areal density fluctuations of up to 50% about the mean for some shots. Clearly, this represent a large, and unacceptable, asymmetry in the imploded fuel.

Motivated by these inferred fuel asymmetries, a dedicated measurement campaign was undertaken after the conclusion of the NIC to measure the in-flight shell asymmetries of NIC-type implosions[15].

Fig. 3 illustrates schematically this technique in which 10 keV x-rays are used to backlight a surrogate capsule implosion. In separate shots, both equatorially and polar images can be taken. An

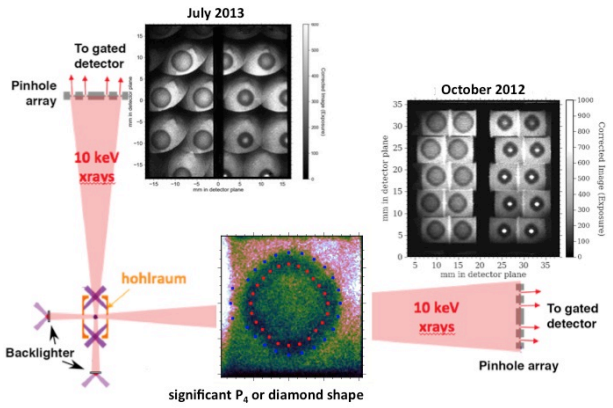

Fig. 3. Schematic of low-mode in-flight asymmetry measurements carried out on NIF

enlarged image of a representative backlit image is shown in the central inset including a fit to the minimum transmission contour (red dots) and the limb minimum (blue dots). Legendre decomposing these fits and comparing to simulations indicated a significant P_4 or diamond-shaped asymmetry in the implosion at a radius of ~ 200 μm. According to simulations, perturbations of this magnitude can be expected to degrade implosion yield by a factor of two[16]. In addition to confirming that unacceptably large low-mode asymmetries were present in NIC implosions, this set of experiments was also able to demonstrate that by lengthening the hohlraum by 700 μm, this P_4 asymmetry could be mitigated and the implosion made round at a radius of ~ 200 μm[17]. Nevertheless, evidence for time-dependent swings in the low-mode symmetry are still present and more refined diagnostics, such as the Advance Radiography Capability (ARC), will be required to diagnose fully the symmetry of the imploded DT fuel.

A second important observation made from these backlit implosion experiments was the unexpectedly large perturbation seeded by the capsule support tent[18]. As shown in Fig. 4, prior to the shot, the capsule is supported in the center of the hohlraum by

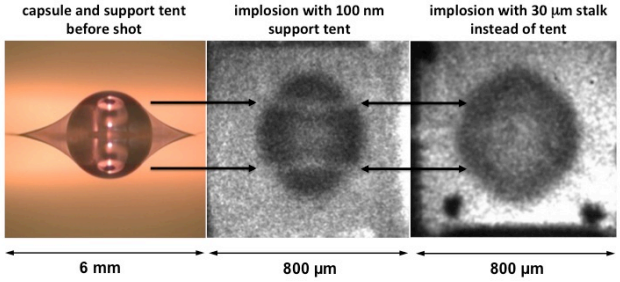

Fig. 4. Illustration of the impact of the capsule support tent as observed by in-flight shell radiography

a pair of thin plastic membranes, referred to as "tents." These tents envelop either pole of the capsule and peal away from the surface of the capsule at a polar angle of roughly 45°. As shown in the middle panel of Fig. 4, this 45° separation point is remarkably coincident with a clear "scar" across the face of the corresponding in-flight radiograph. To confirm that in fact the tent is responsible for this visibly large perturbation, a shot was conducted with the capsule supported by a 30 μm thick stalk as opposed to the conventional tent. While this would seed too large a perturbation to be viable for an ignition capsule at full convergence, the absence of the "tent scar" from this surrogate implosion shown in the right most panel in Fig. 4 clearly confirms that the tent is the source of this perturbation. Following this observation, simulations deliberately perturbed so as to reproduce the radiographic signatures attributed to the tent showed a yield degradation of roughly a factor of two from this effect alone. Note that, in combination with the low-mode shape asymmetries just described, these two effects account for yield degradation of approximately a factor of four, roughly half of the order of magnitude discrepancy observed when comparing post-shot simulations to the data. As a mitigation strategy, successively thinner tents have been used in NIF implosion experiments with the thickness reduced from 110 nm, as used in most NIF shots, down to 45 nm for most recent shots and 15 nm in one demonstration case. Tents thinner than 15 nm appear to be incapable of robustly supporting the capsule, but 15 nm does significantly reduce the perturbation imprinted to the capsule and should be acceptable for achieving ignition.

Evidence suggests that the second large contributor to yield degradation in NIC implosion was mix of ablator material, and possibly cold DT fuel, into the hot spot quenching the yield either by radiative or conductive cooling. The evidence for mix of ablator material into the hot spot is derived from combined measurement of neutron and x-ray yield[19]. In outline, the hot spot x-ray yield is a function of the hot spot density, hot spot temperature, hot spot <*Z*> or contamination fraction, hot spot size, and optical depth of the surrounding ablator. Likewise, the neutron yield of the hot spot is a function again of the hot spot density, hot spot temperature, and hot spot size. Neglecting gradients or other shape details, the ratio of x-ray to neutron yield is then only a function of the hot spot temperature, the optical depth of the surrounding material, and the amount of higher *Z* contamination in the hot spot. Assuming that the hot spot temperature is adequately characterized by the ion temperature inferred from the Doppler width of the emitted neutron spectrum and estimating the ablator optical depth from energy-resolved x-ray emission measurements, the hot spot contamination can then be inferred. A plot of this inferred hot spot contamination or mix mass versus measured neutron yield for a number of NIC shots is shown in Fig. 5. A clear trend of lower yield with higher mix is

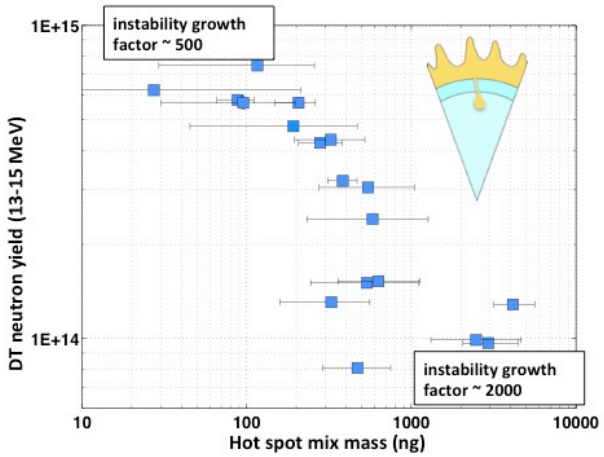

Fig. 5. Correlation of yield degradation with inferred hot spot mix mass from several NIC shots

evident. Also highlighted in Fig. 5 are simulated instability growth factors (ratio of final to initial perturbation amplitudes) for low mix and high mix shots. While the correlation is imperfect, broadly speaking higher mix shots tended to show higher growth factors in simulations and lower mix shots showed lower growth factors. This trend corroborates mix of ablator material into the hot spot as contributing to the observed yield degradations; however, the magnitudes of the hot spot mix shown in Fig. 5 are significantly higher than can be explained by these growth factor estimates. While the trends seem to be understandable from the perspective of design simulations, such heavy contamination of the hot spot is not currently understood.

Like the case of inferred low-mode shape distortions, the evidence for mix in NIC implosions motivated a dedicated campaign to measure the growth of the hydrodynamic instabilities that could generate mix in NIC implosions. The first set of experiments conducted by this "Mix Campaign" was to commission the Hydro Growth Radiography (HGR) platform[20]. This platform uses a standard NIC hohlraum but with the capsule mounted on a reentrant gold cone as shown in Fig. 6. This cone gives access to the interior of the capsule for

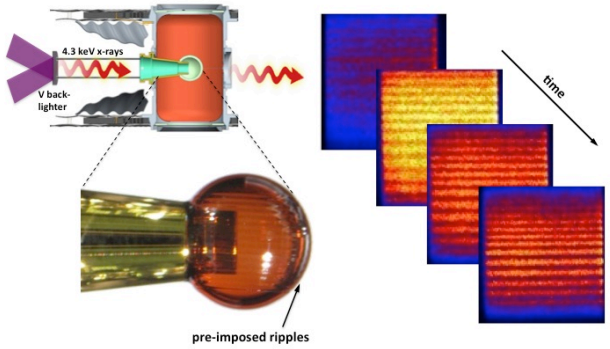

Fig. 6. Schematic representation of the HGR platform

single-pass radiography during the capsule implosion. With perturbations of a known amplitude and wavelength machined onto the surface of the capsule opposite the cone, backlit images provide a direct measure of instability growth factors at the ablation surface on a wavelength-by-wavelength basis. An example of the high quality data generated

by HGR experiments is shown in the right half of Fig. 6. The measured growth factors from these experiments can be distilled into a growth factor spectrum as shown in Fig. 7 and compared to simulations. As shown by the figure, the measurements so far appear to validate the simulation procedure being used to model ablation front instabilities in NIF implosions[21]. A full spectrum of measurements has so far only been made at a convergence of order two, but current plans call for higher convergence measurements as well as measurements of instability growth at other capsule interfaces in addition to the ablation front.

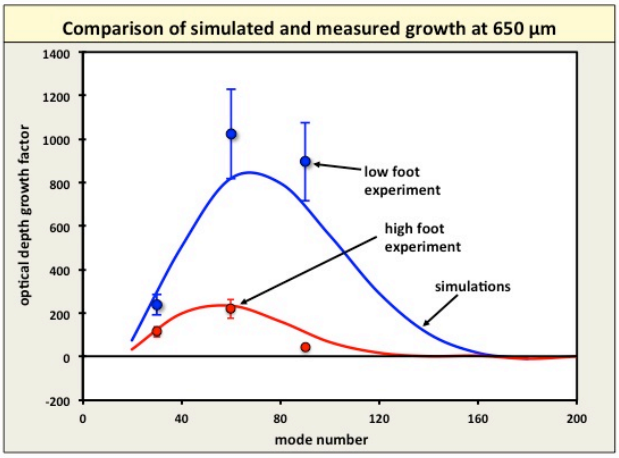

Fig. 7. HGR growth factor data collected at a convergence ratio of approximately two for both low foot (NIC) and high foot implosions

Nevertheless, the apparent agreement between simulated and measured growth rates, as shown in Fig. 7, and the disagreement with inferred mix mass, such as those shown in Fig. 5, leaves a conundrum: How can the simulated growth rates be correct and yet the simulated mix mass, the consequence of these growth factors, be significantly underestimated? Possible answers to this conundrum are that the initial growth seeds are larger than currently believed, or that the later phases of growth beyond what has so far been measured are more rapid than simulated. These hypotheses will be investigated in future experiments. In the near term, however, the inference of larger than expected mix masses motivated a search for implosions designs with significantly reduced instability growth, notably the so-called "high foot" implosion design.

The high foot implosion derived from design studies[22] conducted during the early phases of the NIC in a search for alternate implosion designs with enhanced stability should the planned ignition point[23] design fail due to mix. The essential modification of high foot-type implosion designs is to increase the strength of the first shock launched by the "foot" of the x-ray drive pulse. This higher foot modifies the early-time Richtmyer-Meshkov and ablative Rayleigh-Taylor growth at the ablation front as well as conditioning the ablator such that at late times the ablation front is less compressed and therefore more stable. While modifications to instability growth that could be engineered by modifying the foot of the x-ray pulse had been investigated for some time[24,25], the modification used in the current high foot design comes at the cost of reduced fuel compressibility and hence was not pursued during the NIC. Following the unexplained large amounts of mix encountered in many NIC implosions, however, a more conservative, low-convergence implosion such as the high foot becomes appropriate[26]. Note that these implosion experiments used identical capsules and hohlraums to those fired during NIC; only the laser pulse shape is modified.

Returning to Fig. 2, the encouraging progress of the "High Foot Campaign," as shown by the green points, is evident. The first high foot DT shot was fired on May 1, 2013 using 1.3 MJ and 350 TW[27]. As expected, this implosion produced less compression in the form of a lower areal density (0.6 g/cm^2) than most low-foot implosions, but produced a neutron yield (7.7×10^{14}) comparable to the best performing low foot shots from the NIC. A succession of higher laser power and thinner ablator experiments was then conducted. These experiments culminated in shots in November of 2013 (N131119) and January 2014 (N140120) that crossed the threshold of fuel gains greater than one, *i.e.*, neutron energy yields greater than the kinetic energy coupled to the DT fuel, and showed significant self-heating due to α-particle deposition[28]. Using the full NIF power and energy of 420 TW and 1.9 MJ, N140120 in particular achieved a yield of 9.0×10^{15} at an areal density of 0.8 g/cm^2. That the high foot implosion does produce less ablation front instability growth

than the low foot has also been confirmed in HGR measurements as shown in Fig. 7.

Future plans

With the encouraging results flowing from the high foot implosion campaign, several paths are currently being followed in pursuit of ignition on NIF. These different paths can primarily be grouped around the different ablator options now being pursed in NIF experiments, though each of course has many sub-variants. These ablator candidates and some of their strengths and weaknesses are summarized in Fig. 8.

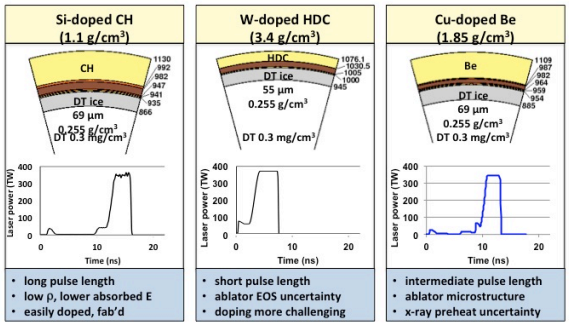

Fig. 8. Trio of ablator types being pursued in current and future NIF ignition experiments

The silicon-doped CH ablators used throughout NIC will continue to be pursued primarily in the context of the high foot campaign. The high foot campaign will continue to investigate further thinning of the ablator to improve implosion velocities, though ultimately this strategy is expected to reintroduce unacceptable levels of mix. Improvements to the low-mode implosion shape will also be pursued as will advanced pulse shaping options that aim to combine the high compression of the low foot with the good ablation front stability of the high foot.

High Density Carbon (HDC) or synthetic diamond, possibly doped with tungsten, has been under active experimental investigation on NIF for the past year. As fabricated, HDC shells are an order of magnitude smoother than CH shells which significantly mitigates instability growth with this ablator. With HDC's higher starting density, it can also be a more efficient absorber of radiation from the hohlraum, leading to higher implosion velocities for the same mass. Current HDC ablator designs are focusing on a two-shock, near-vacuum hohlraum design which experimentally has been shown to reach very high implosion velocities (> 400 km/s); however, low-mode shape in these low gas fill/near-vacuum hohlraums is again proving a challenge.

Finally, beryllium ablator designs are scheduled to be tested on NIF in the near future. The advantages of beryllium as an ablator have long been appreciated, and beryllium has long been considered for NIF ignition implosion designs[29,30]. However, difficulties with uniformly doping beryllium at the time of the NIC as well as concerns over target chamber contamination delayed the exploration of beryllium ablators during the NIC. The currently designs for beryllium ablator experiments are being developed in collaboration with Los Alamos National Laboratory and compare favorably with CH and HDC designs[31,32].

Taken together, these three ablator paths and their sub-variants provide a complimentary set of strengths in pursuit of ignition. In light of experience gained from the NIC, the designs for each are being optimized so as to address the main challenges that foiled ignition during the NIC, namely, larger than expected low-mode shape distortions and higher than anticipated levels of mix into the hot spot. Given the progress achieved so far by the low-mix, high foot implosion platform, the prospects are encouraging that further evolutions of the CH ablator design or one of the alternate HDC or beryllium ablator designs will eventually reach the threshold of propagating thermonuclear burn on NIF.

Acknowledgments

Work performed under the auspices of the U.S. D.O.E. by Lawrence Livermore National Laboratory under Contract No. DE-AC52-07NA27344.

References

1. M. J. Edwards, *et al.*, Phys. Plasmas **20**, 070501 (2013)
2. E. M. Moses, *et al.*, Phys. Plasmas **16**, 041006

(2009)

3. S. Atzeni and J. Meyer-ter-Vehn *The Physics of Inertial Fusion* (Clarendon, Oxford, 2004)
4. C. Cerjan, *et al*., Phys. Plasmas **20**, 056319 (2013)
5. S. H. Glenzer, *et al*., Plasma Phys. Control. Fusion **54**, 045013 (2012)
6. O. Landen, *et al*., Phys. Plasmas **18**, 051002 (2011)
7. M. J. Edwards, *et al*., Phys. Plasmas **18**, 0510013 (2011)
8. A. J. MacKinnon, *et al*., Phys. Rev. Lett. **108**, 215005 (2012)
9. S. H. Glenzer, Phys. Plasmas **19**, 056318 (2012)
10. D. S. Clark, *et al*., Phys. Plasmas **18**, 082701 (2011)
11. V. A. Smalyuk, *et al*., Phys. Rev. Lett. **111**, 215001 (2013)
12. O. S. Jones, *et al*., Phys. Plasmas **19**, 056315 (2012)
13. D. S. Clark, Phys. Plasmas **20**, 056318 (2013)
14. M. M. Marinak, Phys. Plasmas **8**, 2275 (2001)
15. R. P. J. Town, *et al*., Phys. Plasmas, *to appear*
16. A. L. Kritcher, Phys. Plasmas **21**, 042708 (2014)
17. J. R. Rygg, Phys. Rev. Lett, *to appear*
18. S. R. Nagel, *et al*., *in preparation*
19. T. Ma, *et al*., Phys. Rev. Lett. **111**, 085004 (2013)
20. V. A. Smalyuk, *et al*., Phys. Plasmas **21**, 056301 (2013); V. A. Smalyuk, *et al*. Phys. Rev. Lett, *to appear*
21. K. Raman, *et al*., Phys. Plasmas, *to appear*
22. V. N. Goncharov and O. A. Hurricane in *Workshop on the Science of Fusion Ignition on NIF*, San Ramon, CA, May 22 – 24, 2012
23. S. W. Haan, *et al*., Phys. Plasmas **18**, 051001 (2011)
24. D. S. Clark, *et al*., Phys. Plasmas **17**, 052703 (2010)
25. B. A. Hammel, *et al*., High Energy Density Phys. **6**, 171 (2010)
26. T. R. Dittrich, *et al*., Phys. Rev. Lett. **112**, 055002 (2014)
27. H.-S. Park, *et al*., Phys. Rev. Lett. **112**, 055001 (2014)
28. O. A. Hurricane, *et al*., Nature **506**, 343 (2014)
29. D. C. Wilson, *et al*., Phys. Plasmas **5**, 1953 (1998)
30. S. W. Haan, *et al*., Phys. Plasmas **12**, 056316 (2005)
31. A. N. Simakov, *et al*., Phys. Plasmas **21**, 022701 (2014)
32. A. Yi, *et al*., Phys. Plasmas, *to appear*